REFERENCES AND NOTES

1. R. Sonnenfeld and B. C. Schardt, *Appl. Phys. Lett.* **49**, 1172 (1986); P. Lustenberger, H. Rohrer, R. Christoph, H. Siegenthaler, *J. Electroanal. Chem.* **243**, 225 (1988); M. J. Heben, R. M. Penner, N. S. Lewis, M. M. Dovek, C. F. Quate, *Appl. Phys. Lett.* **54**, 1421 (1989).
2. A. M. Mamoon, W. T. Schlapfer, B. H. Fahwiler, C. A. Tobias, *Adv. Biol. Med. Phys.* **16**, 1 (1977); B. Sackmann and E. Neher, *Annu. Rev. Physiol.* **46**, 455 (1984).
3. A. Fitch and D. H. Evans, *J. Electroanal. Chem.* **202**, 83 (1986); W. J. Bower, E. E. Engelman, D. H. Evans, *ibid.* **262**, 67 (1989); C. P. Andrieux, P. Hapiot, J. M. Saveant, *J. Phys. Chem.* **92**, 5987 (1988); *ibid.*, p. 5992.
4. C. W. Lin, F. R. Fan, A. J. Bard, *J. Electrochem. Soc.* **134**, 1038 (1987); D. H. Craston, S. W. Lin, A. J. Bard, *ibid.* **135**, 785 (1988); J. Schneir *et al.*, *Proc. SPIE* **897**, 16 (1988).
5. D. O. Wipf, E. W. Kristensen, M. R. Deakin, R. M. Wightman, *Anal. Chem.* **60**, 306 (1988).
6. D. O. Wipf and R. M. Wightman, *ibid.*, p. 2460; C. P. Andrieux, D. Garreau, P. Happiot, J. Pinson, J. M. Saveant, *J. Electroanal. Chem.* **243**, 321 (1988).
7. P. T. Kissinger, J. B. Hart, R. N. Adams, *Brain Res.* **55**, 209 (1973); J. C. Conti, E. Strope, R. N. Adams, C. A. Marsden, *Life Sci.* **23**, 2705 (1978); A. G. Ewing, R. M. Wightman, M. A. Dayton, *Brain Res.* **249**, 361 (1982).
8. K. Tanaka and N. Kashiwagi, *Bioelectrochem. Bioenerg.* **17**, 519 (1987); *ibid.* **21**, 95 (1989).
9. E. Neher and B. Sackman, *Nature* **260**, 779 (1976); ———, J. H. Steinbach, *Pfluegers Arch. Gesamte Physiol. Menschen Tiere* **375**, 219 (1978); F. Conti and E. Neher, *Nature* **285**, 140 (1980).
10. R. A. Wallingford and A. G. Ewing, *Anal. Chem.* **60**, 1972 (1988); *ibid.*, p. 258.
11. J. Duke, E. R. Scott, H. S. White, *J. Electroanal. Chem.* **264**, 281 (1989).
12. M. Fleischmann, S. Pons, D. R. Rolison, P. P. Schmidt, *Ultramicroelectrodes* (Datatech Systems, Morgantown, NC, 1987), chap. 3.
13. M. J. Heben, M. M. Dovek, N. S. Lewis, R. M. Penner, C. F. Quate, *J. Microsc.* **152**, 651 (1988); M. J. Heben, thesis, California Institute of Technology (1990).
14. R. M. Penner, M. J. Heben, N. S. Lewis, *Anal. Chem.* **61**, 1630 (1989).
15. M. L. Wolbarsht, E. F. MacNichol, Jr., H. G. Wagner, *Science* **132**, 1309 (1960); C. Guld, *Med. Electron. Biol. Eng.* **2**, 317 (1964).
16. W. H. Reinmuth, *J. Am. Chem. Soc.* **79**, 6358 (1957).
17. M. A. Dayton, J. C. Brown, K. J. Stutts, R. M. Wightman, *Anal. Chem.* **52**, 946 (1980).
18. A. J. Bard and L. R. Faulkner, *Electrochemical Methods* (Wiley, New York, 1980), chaps. 5, 6, 8, and 9.
19. Experimental problems associated with the determination of k_{het} with cyclic voltammetry, for example, are discussed in the following references: D. F. Milner and M. J. Weaver, *Anal. Chem. Acta* **198**, 245 (1987); J. O. Howell, W. G. Kuhr, R. E. Ensman, R. M. Wightman, *J. Electroanal. Chem.* **209**, 77 (1986); A. M. Bond *et al.*, *Anal. Chem.* **60**, 1878 (1988).
20. A. Russell *et al.*, *Anal. Chem.* **58**, 2961 (1986); K. B. Oldham, C. G. Zoski, A. M. Bond, D. A. Sweigart, *J. Electroanal. Chem.* **248**, 467 (1988).
21. Z. Galus, J. Golas, J. Osteryoung, *J. Phys. Chem.* **92**, 1103 (1988).
22. K. B. Oldham and C. G. Zoski, *J. Electroanal. Chem.* **256**, 11 (1988).
23. M. J. Weaver and T. L. Satterberg, *J. Phys. Chem.* **81**, 1772 (1977); M. J. Weaver, *J. Electroanal. Chem.* **93**, 231 (1978); T. L. Satterberg and M. J. Weaver, *J. Phys. Chem.* **82**, 1784 (1978); S. W. Barr, K. L. Guyer, M. J. Weaver, *J. Electroanal. Chem.* **111**, 41 (1980).
24. T. Gennett and M. J. Weaver, *Anal. Chem.* **56**, 1444 (1984).
25. A. M. Bond *et al.*, *ibid.* **60**, 1878 (1988).
26. R. B. Morris, D. J. Franta, H. S. White, *J. Phys. Chem.* **91**, 3559 (1987).
27. R. A. Marcus, *ibid.* **67**, 853 (1963); R. A. Marcus, *Annu. Rev. Phys. Chem.* **15**, 155 (1964).
28. T. Saji, T. Yamada, S. Aoyagui, *J. Electroanal. Chem.* **61**, 147 (1975); T. Saji, *ibid.* **86**, 219 (1978).
29. J. Silverman and R. W. Dodson, *J. Phys. Chem.* **56**, 846 (1952).
30. B. S. Brunschwig, C. Creutz, D. H. Macartney, T. K. Sham, N. Sutin, *Faraday Discuss. Chem. Soc.* **74**, 113 (1982).
31. J. T. Hupp and M. J. Weaver, *J. Phys. Chem.* **93**, 4703 (1989).
32. T. J. Meyer and H. Taube, *Inorg. Chem.* **7**, 2369 (1968).
33. R. M. Neilson, G. E. McMannis, L. K. Safford, M. J. Weaver, *J. Phys. Chem.* **93**, 2152 (1989).
34. R. M. Neilson, G. E. McMannis, M. J. Weaver, *ibid.*, p. 4703.
35. C. R. Bock *et al.*, *Chem. Phys. Lett.* **61**, 522 (1979).
36. Z. Samec and J. Weber, *J. Electroanal. Chem.* **77**, 163 (1977).
37. D. H. Angell and T. Dickinson, *ibid.* **35**, 55 (1972).
38. M. I. Montenegro and D. Pletcher, *ibid.* **200**, 371 (1986).
39. We acknowledge the Office of Naval Research for support of this work and F. C. Anson and M. J. Weaver for helpful discussions. Contribution no. 8153 from the Division of Chemistry and Chemical Engineering at Caltech. We dedicate this report to George McManis, whose promising scientific career was tragically cut short by his untimely death.

15 August 1990; accepted 13 September 1990

Simulations of the Folding of a Globular Protein

JEFFREY SKOLNICK AND ANDRZEJ KOLINSKI

Dynamic Monte Carlo simulations of the folding of a globular protein, apoplastocyanin, have been undertaken in the context of a new lattice model of proteins that includes both side chains and α-carbon backbone atoms and that can approximate native conformations at the level of 2 angstroms (root mean square) or better. Starting from random-coil unfolded states, the model apoplastocyanin was folded to a native conformation that is topologically similar to the real protein. The present simulations used a marginal propensity for local secondary structure consistent with but by no means enforcing the native conformation and a full hydrophobicity scale in which any nonbonded pair of side chains could interact. These molecules folded through a punctuated on-site mechanism of assembly where folding initiated at or near one of the turns ultimately found in the native conformation. Thus these simulations represent a partial solution to the globular-protein folding problem.

THE SOLUTION TO THE PROTEIN folding problem should not only provide the folded native conformation of a protein, but also information on the mechanism by which a protein attains the folded configuration (*1–3*). Proteins do not fold by a random search (*3*). The observed folding times are on the order of seconds or minutes (*1, 4*), and a random search of all configurations by a small protein of 100 residues would take at least 10^{50} years (*3*). Unfortunately, because of the size of proteins and the time scale of folding, simplified models must be used to make the folding algorithms practical. One such simplification is to use a lattice (*5*). We describe results on a new class of lattice models applied to the folding, from randomly generated, unfolded conformations, of a 99-residue Greek key β-barrel protein, apoplastocyanin (*6*). The native structure is topologically similar to the nuclear magnetic resonance (NMR) solution structure of french bean Cu(I) plastocyanin (*7*) and the x-ray crystal structure of apopoplar plastocyanin (*8*), and differs only in local detail because of the small side-chain representation used in this preliminary study.

Lattice representations of proteins have a long history (*5, 9*). Recently Dill and coworkers (*10, 11*) exhaustively searched the sequence and conformational space of compact polymers and found that compactness induces secondary structure. These studies are complementary to the present work, which allows the examination of longer and more realistic chains, and where folding-pathway information is also obtained. However, the more realistic approach precludes an exhaustive sequence and conformational search.

For highly simplified diamond lattice models, we addressed the requirements to uniquely obtain the native state for model α-helical (*12*) and β-sheet proteins (*13, 14*) and also examined their folding pathways (*15, 16*). While a diamond lattice can perhaps provide general insights into the folding process, it poorly represents local secondary structures. Thus a different lattice must be used if proteins are to be treated in greater detail.

The new lattice model of globular proteins provides a good local description of the protein backbone conformation and yet remains computationally tractable. The entire space is embedded into an underlying cubic lattice where adjacent lattice sites are a dis-

J. Skolnick, Department of Molecular Biology, Research Institute of Scripps Clinic, La Jolla, CA 92037.
A. Kolinski, Department of Chemistry, University of Warsaw, 02-093 Warsaw, Poland.

tance of unity apart. The three-dimensional (3-D) structure of the protein is specified by both the α-carbon backbone and β-carbon side positions of each residue (*17*). The centers of adjacent α-carbons of the protein backbone are connected by a vector of the type (±2, ±1, 0). Therefore, this is called a "210 lattice," and the α-carbons are connected by the 3-D generalization of a "knight's walk" in chess. If physically realistic distances between second-nearest neighbors are allowed, each α-carbon has 18 accessible internal conformational states. The surrounding six neighboring sites of each α-carbon are also occupied to implement the finite backbone thickness. Since multiple occupation of any lattice site is rigorously prohibited, this procedure mimics the hard-core repulsive region of the protein backbone rather well. In addition, there is a soft-core repulsion between α-carbons that extends up to 1.7 Å, and hydrogen-bond–type interactions are included. Except for glycines, which are devoid of side chains, all side chains have approximately the volume of a methyl group, have *l*-chirality, and have a surface defined by four lattice sites. Three sites are connected to the α-carbon by a face-centered cubic lattice (fcc)–type vector [a vector of the form (±1, ±1, 0)], and the fourth site, which is the center of the tertiary interaction, is connected to the α-carbon by a vector of the type (±1, ±1, ±1). As the conformation of the backbone changes, the side chains also change orientation. The backbone conformation is modified by a series of local elemental jumps as well as by moves that can translate and rotate arbitrary portions of the chain (*13, 18*). The latter serve to move about assembled elements of secondary structure. The acceptance of the moves is based on an asymmetric Metropolis scheme (*19, 20*), and the conformations are sampled by using Monte Carlo dynamics (*20*). In each elemental time unit, every bead on average is subjected to local modifications involving a spike move and several attempts at secondary structure translations and rotations. Typically, at high temperature, about 17% of the local spike moves, 3% of the large-scale rotations, and 0.03% of the large-scale translations succeeded. The set of moves we used generated correct local and global dynamics for the denatured state (*21, 22*), and thus it may provide insights into the nature of the folding pathways (*15, 16*).

The full amino acid sequence is used, and tertiary interactions between any spatially close (and not necessarily native) pair of side chains are implemented with a modified Miyazawa-Jernigan (MJ) hydrophobicity scale (*23*) for interresidue contact energies.

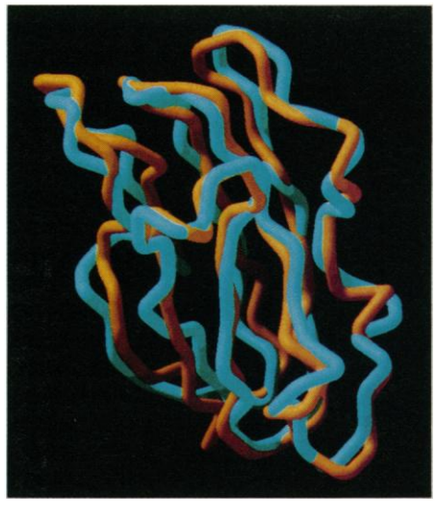

Fig. 1. The NMR solution structure of french bean plastocyanin in red and the corresponding superimposed lattice fit of apoplastocyanin in blue.

This scale is based on the frequency of occurrence of interresidue contacts in protein crystal structures. The interaction between side chains is independent of the backbone conformation. Covell and Jernigan (*24*) used the MJ scale to order compact conformations generated by an exhaustive search. They find for the five proteins studied that the native conformation is always within the best 2% of all generated conformers; this agreement provides confidence that the MJ scale can provide a reasonable first estimate of the relative ordering of interresidue contact energies.

Since the MJ parameterization is in the natural language of a lattice model, it is the first of a number of such scales to be used. Miyazawa and Jernigan found a linear relation between average contact energies for nonpolar residues and the Nozaki-Tanford hydrophobicity scale (*25*), although the MJ values are about twice as large. Direct application of the MJ scale gave contact energies on the order of 10 to 15 k_BT (thermal energy) in the calculated thermal transition region; these values are far too large. To alleviate this problem, the contact pair energies were uniformly scaled by a factor of 0.15. This procedure provides a Leu-Leu interaction energy in reasonable agreement with that extracted from fitting a statistical mechanical theory of the helix-coil transition of two-chain, coiled coils (*26*) to the thermal transition of synthetic tropomyosin analogs (*27*).

The local intrinsic conformational propensities for each residue must be assigned. In the model, for the *i*th residue this translates into preferences for distances between α-carbons $i - 1$ and $i + 1$, the distance between α-carbons $i - 1$ and $i + 2$, and the chirality of three consecutive α-carbon bonds. As a first approximation, the local conformational preferences are taken to be consistent with the folded conformation. By recognizing that this is a rotational isomeric states model (*17*), an analytic theory has been constructed that estimates the location of the transition region as a function of temperature (*15, 18*). The theory gives results within 3% of the simulated value for the transition midpoint. This theory also allows for an estimate of the population of the native state based on these local preferences alone; typically, populations of 10^{-25} are obtained. In other words, non-native conformations are overwhelmingly preferred. Thus the native state is definitely not enforced by the local preferences, and a range of values have been tried, all of which yielded successful folding events. The contribution to the native energy due to local preferences ranges from 1/3 to 3/4 of the total. In the example described below, at the estimated transition midpoint, the total native-state energy is $-236.9\ k_BT$, of which local interactions contribute $-179.5\ k_BT$, side-chain interactions contribute $-44.1\ k_BT$, and hydrogen-bond–type interactions contribute $-13.3\ k_BT$.

The ability of 210 lattice model to approximate the native conformation of real globular proteins was tested by fitting 64 proteins in the Brookhaven Protein Data Bank to the lattice, including multiple-domain proteins. We obtained a root-mean-square (rms) deviation of 1.9 Å between the α-carbons of the lattice model and the crystal structures. Since rms values alone can be misleading, we show an example (Fig. 1) of the NMR solution structure of french bean plastocyanin (*7*) in red and the corresponding superimposed 210 lattice fit to apoplastocyanin in blue. In this lattice representation, excluded volume restrictions were rigorously enforced. The rms deviation between α-carbons is 1.7 Å.

French bean plastocyanin has been chosen in this first application of the 210 lattice model because the Greek key β barrel (Fig. 1) topology reverses strand direction (*6*). Labeling the strands from the amino terminus, the carboxyl-terminal strands 7 and 8 close the β barrel and pack against the amino-terminal strands 1, 2, and 3; the latter triplet also reverses strand direction. Thus this topology is a good test of the efficiency of the folding algorithm.

A major limitation of our side-chain representation is that while the side chains are not uniform in interaction, they are uniform in size and too small. Thus, to generate a densely packed protein core, the best lattice approximation to the native plastocyanin was subjected to Monte Carlo dynamics

(*20*). This procedure produced a family of dense conformations, each topologically identical with the real plastocyanin; the lowest energy conformation was chosen as native. The resulting "crumpled" plastocyanin has a rms of 6.1 Å from the best lattice fit to real plastocyanin and is shown in stereo in Fig. 2, in yellow, superimposed on the best lattice fit, shown in blue. The "crumpled" plastocyanin is topologically similar to the NMR solution structure and constitutes the "native" conformation in the model. The mean-square-radius of gyration, $\langle S^{2}{}_{N} \rangle$, of idealized (best lattice fit) native plastocyanin is 151.2 Å^2 (150.7 Å^2).

The probability of finding a native turn or loop in the denatured state reflects on whether the native turns and loops are enforced. Recently, Dyson *et al.* (*28*) used two-dimensional NMR to examine fragments of french bean plastocyanin encompassing the loop and turn regions of the native molecule and found a negligible intrinsic propensity for all native loop and turn conformers. This result is in excellent agreement with the conditions required to fold the model plastocyanin where residues 31 to 35 have an intrinsic loop population of ~3% and, consistent with the NMR studies, comprise the most populated loop or turn region. The remainder of the loops and bends have native conformations that are about an order of magnitude less populated. This result was independently established without prior knowledge of the NMR results and is based entirely on the requirements to obtain the idealized native plastocyanin conformation on successive refolding. Thus the simulation requires a set of parameters that result in marginal native-turn propensities that are in accord with experiment.

In a total of at least eight independent renaturation runs for each particular set of parameters, the native conformation has been obtained each time. Three different parameter sets were tried, that differed in the ratio of the stabilities of the turns, the amino- versus carboxyl-terminal regions of the molecule, and the particular realization of the native state. For the situation described in detail below, the native conformation was obtained in all ten renaturation attempts. For the other two sets of parameters, the native conformation was obtained in eight of eight and ten of ten cases, respectively.

Starting from a randomly generated denatured state, the model protein was systematically cooled into the transition region. For each temperature, the system was allowed to equilibrate. At high temperature, random coil conformations were sampled. On further cooling, an all-or-none transition to the native state occurred (*29*). The number of native contact pairs between side chains versus time at a fixed temperature obtained over an entire folding trajectory is shown in Fig. 3A. (There are 34 in the fully folded conformation.) Thus these systems reproduce the thermodynamics of real, small globular proteins (*1, 29*). Furthermore, an all-or-none transition is not an intrinsic feature of these algorithms, which yield a continuous transition when appropriate (*13, 17*). In the transition region, the system undergoes reversible folding and unfolding. At lower temperatures, apart from some minor tail thrashing, the native conformation is very stable. The elapsed folding time from the first appearance of secondary structure that persisted until the successful completion of folding was 3,285,000 time steps.

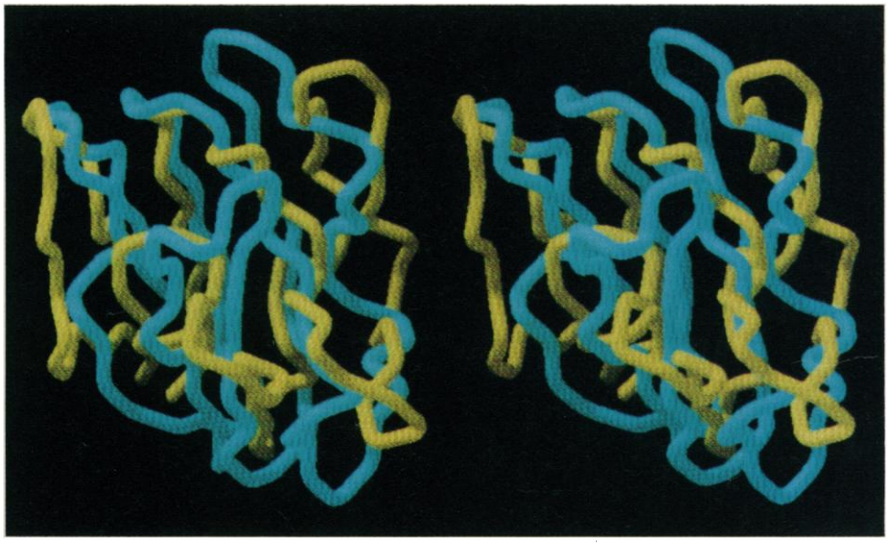

Fig. 2. "Crumpled" apoplastocyanin structure in yellow and the best lattice fit to apoplastocyanin in blue.

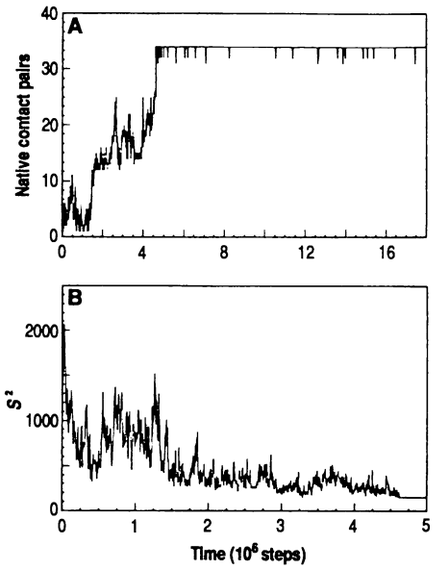

Fig. 3. For a representative folding trajectory, (**A**) a plot of the number of contacts between pairs of side chains versus time and (**B**) the instantaneous value of the square of the radius of gyration S^2 versus time.

This trajectory is further examined in Fig. 3B, where the instantaneous value of the square of the radius of gyration, S^2, is plotted versus time; $\langle S^2 \rangle$ for the denatured state is 875.8 Å^2. Initially there were wide-ranging fluctuations characteristic of the denatured state. Folding initiated at t = 1,340,000 (see below) and was accompanied by a substantial diminution in the values of S^2. In the latter stages of folding, S^2 further decreased, with the average value from t = 3,000,000 until folding ended at t = 4,625,000 equal to 278.3 Å^2. In many respects, these late-folding intermediates have many properties of the putative molten globule state (*3*). They are compact and exhibit substantial secondary and tertiary structure, with the latter in particular experiencing substantial fluctuations (*30*).

Selected portions of a representative folding trajectory are examined in Fig. 4 to determine the nature of these folding intermediates. In this, as in all runs, the system experienced many unsuccessful attempts at initiation prior to a successful folding event. The first element of secondary structure that persisted until the end of folding was turn 4, first observed at t = 1,340,000. In this conformation, two of the total of four pairs of side-chain contacts are native. Although the Monte Carlo moves could in principle move about assembled elements of secondary structure, folding occurred by on-site construction. At t = 1,440,000, native turn 5 first appeared and was followed by the formation of native turn 3 at t = 1,880,000. At t = 2,325,000, native turn 3 dissolved, but reformed by t = 2,330,000. The next ele-

ment of secondary structure that appeared was loop 6; this conformation persisted from t = 2,445,000 until t = 2,660,000. During the intervening time, β strands 7 and 8 formed on-site, and as shown at t = 2,660,000, the entire carboxyl-terminal portion of the molecule assembled. Immediately following this snapshot, β strand 8 and turn 7 dissolved. In fact, β strand 7 and 8 dissolved and reformed many times; one such conformation at t = 2,920,000 is shown. Thus folding was not unidirectional. Loop 6 was fixed in place at t = 3,930,000. The final time turn 7 reformed was at t = 4,415,000. Turn 2 formed at t = 4,550,000, where nonnative conformations of the amino-terminal portion are still evident. By t = 4,615,000, β strand 2 formed by on-site construction. Native turn 1 and β strand 1 formed by t = 4,620,000, and the fully native molecule was recovered for the first time at t = 4,625,000. Thus, consistent with Fig. 3A, assembly was followed by punctuation, as the tails thrashed about trying to find conformations consistent with the native state. The partially native molecule comprised of β strands 3, 4, and 6 and helix 5 persisted for 2,030,000 out of the 3,285,000 time steps it took for the protein to fold.

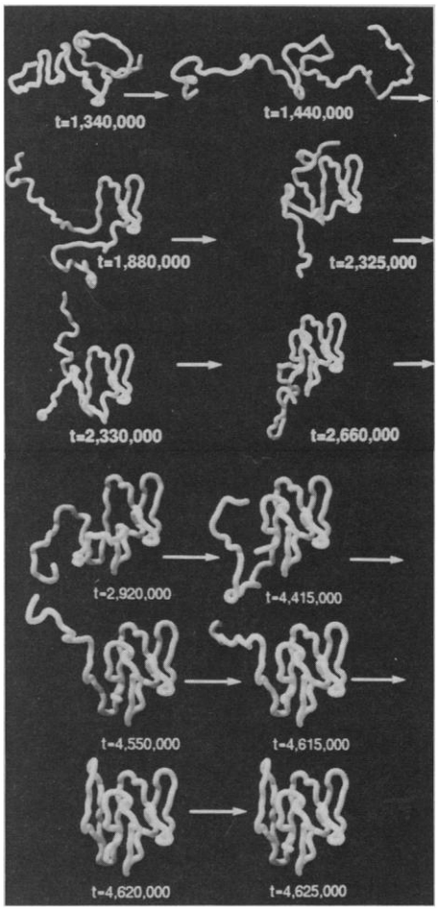

Fig. 4. The identical folding trajectory as in Fig. 3 is used. Representative snapshots show crucial points along the folding pathway.

Turn 4 (residues 47 to 50) was the folding initiation site in all but one of the successful trajectories (27 of 28). In that case, turn 5 (residues 61 to 64) appeared first, which occurred primarily because plastocyanin is a Greek key sandwich of two β sheets (*8*). The packing and interaction of sheet 4 was better with the neighboring helix 5 than it was with sheet 3 in our realization.

There are a multiplicity of folding pathways. In six of the ten cases for this set of parameters, the amino-terminal portion assembled last, and in the other four cases, it was the carboxyl-terminal portion. The observed pathways in order of appearance of the turns that survived until the native state fully assembles are summarized in Table 1, where results from all three parameter sets are included. Consistent with experiment, the relatively long-lived intermediates possess a substantial amount of secondary and tertiary structure and lie closer to the folded rather than the denatured state (*2*).

Because of the poor side-chain packing, it was substantially more difficult to fold these "crumpled" molecules than it would be when more realistic side chains are used. Thus the ability to fold to the crumpled plastocyanin native state is a rather severe test of the folding algorithm. Furthermore, the relative lifetimes of the folding intermediates may partially reflect artifacts of the model. To substantiate this, we also constructed a regularized version of model plastocyanin in which the conformation is consistent with the small side-chain representation. Two kinds of residues, hydrophilic and hydrophobic, were used. Qualitatively identical folding pathways to those found here are observed. However, folding is a factor of 3 to 10 faster than in the crumpled plastocyanin case. Furthermore, the pathway with the carboxyl-terminal end assembling last was also observed in a diamond lattice model of plastocyanin (*15*). Successful folding has also been obtained where the putative β regions locally favor α helix. These results suggest that the simulated pathways are characteristic of topology alone and are independent of lattice and model realization, and therefore provide encouragement that they may be physical.

On going from a diamond lattice model to the 210 lattice model, there are 6^{n-3} additional configurational degrees of freedom. Thus, if the algorithm hunted through all of the configuration space to solve the folding problem, the 210 lattice model would be computationally intractable. The elapsed time from successful folding initiation until the native Greek key was obtained is about a factor of 100 longer on the 210 lattice than on the diamond lattice (*15*). Thus, both systems exhibit a relatively efficient means of partitioning configuration space. They do so by initiating folding at or near turns. However, in the β protein considered here, the residues involved in the turns needed only have a marginal, intrinsic native turn preference. These algorithms solved the folding problem by using assembled elements of tertiary structure to reduce the search through configuration space by the remaining unfolded portions of the chain. Thus, a β strand built onto an adjacent strand that had already assembled. When the direction reversed, as on going from strand 6 to 7, then the unassembled random-coil tail rattled around until it found the hydrophobic face onto which it subsequently attached. Here, the existing tertiary structure hindered assembly; often, the unassembled tail was left dangling until it eventually worked its way under or around the molecule and then assembled. Assembly seemed to alternate between periods of rapid construction, followed by a pause each time an unassembled tail exited a β sheet or an α helix and encountered regions that had a weak intrinsic preference to form turns or loops.

The present series of simulations has demonstrated that starting from a marginal intrinsic propensity for secondary structure consistent with the native state (helices and sheet conformations locally can be made isoenergetic or even locally favor the wrong secondary structure) and a full set of tertiary interactions, the native topology of a real protein can be reproducibly folded. If folding using a set of local propensities consistent with, but by no means enforcing the native conformation did not occur, then our whole method of approach to the folding problem would have to be seriously questioned. However, the approach has worked

Table 1. Observed folding pathways.

Number of examples	Order of occurrence of turns t and loops*
10	$t_4 \rightarrow t_5 \rightarrow t_6 \rightarrow t_7 \rightarrow t_3 \rightarrow t_2 \rightarrow t_1$
4	$t_4 \rightarrow t_3 \rightarrow t_2 \rightarrow t_1 \rightarrow t_5 \rightarrow t_6 \rightarrow t_7$
4	$t_4 \rightarrow t_5 \rightarrow t_3 \rightarrow t_6 \rightarrow t_7 \rightarrow t_2 \rightarrow t_1$
2	$t_4 \rightarrow t_5 \rightarrow t_6 \rightarrow t_3 \rightarrow t_7 \rightarrow t_2 \rightarrow t_1$
1	$t_4 \rightarrow t_5 \rightarrow t_6 t_3 t_7 \rightarrow t_2 \rightarrow t_1$
3	$t_4 \rightarrow t_5 \rightarrow t_6 \rightarrow t_3 \rightarrow t_2 \rightarrow t_1 \rightarrow t_7$
1	$t_4 \rightarrow t_5 \rightarrow t_3 \rightarrow t_2 \rightarrow t_1 \rightarrow t_6 \rightarrow t_7$
1	$t_4 \rightarrow t_3 \rightarrow t_5 \rightarrow t_2 \rightarrow t_1 \rightarrow t_6 \rightarrow t_7$
1	$t_4 \rightarrow t_3 \rightarrow t_2 \rightarrow t_5 \rightarrow t_6 \rightarrow t_7 \rightarrow t_1$
1	$t_5 \rightarrow t_4 \rightarrow t_3 \rightarrow t_2 \rightarrow t_1 \rightarrow t_6 \rightarrow t_7$

*Taken from successful folding trajectories where a given turn or loop appeared and persisted to the end of the folding.

and reproduced many qualitative experimental features.

REFERENCES AND NOTES

1. T. E. Creighton, *J. Phys. Chem.* **89**, 2452 (1985).
2. _____, *Proc. Natl. Acad. Sci. U.S.A.* **85**, 5082 (1988).
3. C. Levinthal, *J. Chim. Phys.* **65**, 44 (1968).
4. R. L. Baldwin, *Annu. Rev. Biochem.* **44**, 453 (1975).
5. N. Gō, H. Abe, H. Mizuno, H. Taketomi, *Protein Folding*, N. Jaenicke, Ed. (Elsevier/North-Holland, Amsterdam, 1980), pp. 167–181.
6. J. Richardson, *Adv. Protein Chem.* **34**, 167 (1981).
7. W. J. Chazin and P. E. Wright, *J. Mol. Biol.* **202**, 623 (1988); J. M. Moore, G. P. Gippert, D. A. Case, P. E. Wright, unpublished results.
8. J. M. Guss and H. C. Freeman, *J. Mol. Biol.* **169**, 521 (1983); J. M. Guss, P. R. Harrowell, M. Murata, V. A. Norris, H. C. Freeman, *ibid.* **192**, 361 (1986).
9. H. Taketomi, F. Kano, N. Gō, *Biopolymers* **27**, 527 (1988).
10. H. C. Chan and K. A. Dill, *Macromolecules* **22**, 4559 (1989).
11. K. F. Lau and K. A. Dill, *Proc. Natl. Acad. Sci. U.S.A.* **87**, 638 (1990).
12. A. Sikorski and J. Skolnick, *ibid.* **86**, 2668 (1989).
13. J. Skolnick, A. Kolinski, R. Yaris, *Biopolymers* **28**, 1059 (1989).
14. _____, *Proc. Natl. Acad. Sci. U.S.A.* **86**, 1229 (1989).
15. J. Skolnick and A. Kolinski, *J. Mol. Biol.* **212**, 787 (1990).
16. A. Sikorski and J. Skolnick, *ibid.*, p. 819.
17. P. Flory, *Statistical Mechanics of Chain Molecules* (Interscience, New York, 1969), chap. 7.
18. J. Skolnick and A. Kolinski, unpublished results.
19. N. A. Metropolis, A. W. Rosenbluth, M. N. Rosenbluth, A. H. Teller, E. Teller, *J. Chem. Phys.* **21**, 1087 (1953).
20. K. Binder, *Monte Carlo Methods in Statistical Physics*, K. Binder, Ed. (Springer-Verlag, Berlin, 1987), pp. 1–45.
21. A. Baumgartner, *Annu. Rev. Phys. Chem.* **35**, 419 (1984).
22. G. Nielsen, A. Sikorski, A. Kolinski, J. Skolnick, unpublished results.
23. S. Miyazawa and R. L. Jernigan, *Macromolecules* **18**, 534 (1985).
24. D. G. Covell and R. L. Jernigan, *Biochemistry* **29**, 3287 (1990).
25. Y. Nozaki and C. Tanford, *J. Biol. Chem.* **246**, 2211 (1971).
26. A. Holtzer and J. Skolnick, *Biopolymers* **27**, 87 (1988).
27. S. Y. M. Lau, A. K. Taneja, R. S. Hodges, *J. Biol. Chem.* **259**, 13253 (1986).
28. H. J. Dyson, J. R. Sayre, R. A. Lerner, P. E. Wright, unpublished results.
29. P. Privalov, *Adv. Protein Chem.* **33**, 167 (1979).
30. D. A. Dolgikh *et al.*, *FEBS Lett.* **136**, 311 (1981).

31. Stimulating discussions with J. Dyson, L. Walters, R. A. Lerner, and P. E. Wright are gratefully acknowledged. We thank M. Pique for assistance with computer graphics, and V. Taurasi for preparation of the manuscript.

17 May 1990; accepted 24 August 1990

Scaling Population Density to Body Size in Rocky Intertidal Communities

PABLO A. MARQUET,* SERGIO A. NAVARRETE,† JUAN C. CASTILLA

Interspecific comparisons of animal population density to body size has been the subject of active research in the last decade, especially for terrestrial animals when considering particular taxa or taxonomic assemblages. Studies of rocky intertidal communities showed that animal population density scales with body size to the −0.77 power. This relation held within local communities representing a broad array of animal taxa and was not affected by a dramatic alteration in the network of between-species interactions, as revealed by two long-term human exclusion experiments.

THE RELATION BETWEEN POPULATION density and body size (scaling) has been investigated primarily in terrestrial habitats, with a strong taxonomic bias toward related species (*1–3*). Natural communities, that is assemblages of species populations that co-occur in space and time (*4*), have not been well studied. Reconstructed taxonomic assemblages (*5*) formed by the compilation of published data on particular groups of related species have frequently been used. Because the species come from communities in which the degrees of biotic and abiotic influences are not known, it is not possible to assess the effect of present-day ecological processes on the statistical pattern shown between body size and population density. However, despite these constraints, explanations of the population scaling, based on the action of competition and predation, have been advanced (*1, 6, 7*).

We focused on natural communities that include species in distantly related taxa. In this way, we can set aside evolutionary constraints imposed by phylogenetic similarity and examine constraints imposed by ecological interactions on a local scale. This makes it possible to assess the effect of ecological processes on the interspecific relation between population density and body size. We used data from natural rocky intertidal communities in central Chile to obtain the general relation between population density and body size for invertebrates, and then we tested the effects that markedly different community structures exert on such a relation.

The study sites were located at two marine preserves, Las Cruces and Montemar, from which man has been excluded for an extended time (*8*). These two large-scale long-term experiments of human exclusion produced alterations in the species interaction network, which in turn resulted in dramatic and persistent changes in the intertidal landscape (*9*). Inside the marine preserves the substratum is dominated by chthamaloid barnacles and outside by mussel beds. Moreover, as a result of human exclusion, sizes and densities of algae, herbivores, and predators also differ from inside and outside the preserves (*9–10*). By comparing the scaling of population density with body size between the communities inside and outside each marine preserve, the effects of present-day ecological differences (*10*) could be assessed.

At Las Cruces and Montemar, we selected by chance ten transects inside the marine preserves and ten outside. Ecological population density (*11*) and mean body length of the species included in the analysis (*12*) were evaluated along each transect. Body weights were obtained from regression analysis with weight and length data (*13*).

The relation of population density and body size for data pooled from outside and inside the two marine preserves is shown in Fig. 1. Body size explains a significant amount of the variation observed in population density [$F(1,46) = 50.8$; $P = 0.0001$]. The relation is characterized by a slope of -0.77 (SE = 0.11), which is not significantly different from the slope of -0.75 reported for terrestrial animals (*1, 14*). This similarity expands the generality of this relation, despite known ecological differences between these two systems (*15*). The observation of this relation in intertidal systems, where usually space is a limiting resource for sessile species, suggests that explanations based on energetic constraints acting through differences in the per capita use of a limited resource, such as food (*6*), are not completely satisfactory. A similar point has been raised by Gaston and Lawton (*7*) for bracken herbivores.

In Fig. 2, the relation with the same species inside and outside of each marine preserve is shown. Although the community structures differ inside and outside the preserves (*9*), their characteristic scalings of population density with body size were not significantly different (*16*). This result gives a strong basis to suggest that the population

Departamento de Ecología, Facultad de Ciencias Biológicas, Universidad Católica de Chile, Casilla 114-D, Santiago, Chile.

*Present address: Department of Biology, University of New Mexico, Albuquerque, NM 87131.
†Present address: Department of Zoology, Oregon State University, Corvallis, OR 97331–2914.